Experimental Evaluation and Theoretical Study of Imidazolium and Benzimidazolium Derivatives as Corrosion Inhibitors of Mild Steel in a 0.5 M H_2SO_4 Solution

Mohamed Elhadi Said[1,2], Mehdi Bouchouit[1], Abdellah Zaiter[1,3], Bilel Mezhoud[1], Sofiane Bouacida[1], Aissa Chibani[1] and Abdelmalek Bouraiou[1*]

[1]Unit for Environmental Chemistry and Molecular Structural Research, CHEMS, University of Frères Mentouri, Constantine, Algeria
[2]Faculty of Technology, P. O. Box 166, University Mohamed Boudief M'ila, 28000, Algeria
[3]Laboratory of Applied Chemistry and Matherials Tecnhology, University of Larbi Ben M'Hidi, 04000, Oum El Bouaghi, Algeria
[*]Corresponding author:bouraiou.abdelmalek@yahoo.fr

Received 28/09/2021; accepted 05/01/2022
https://doi.org/10.4152/pea.2023410201

Abstract
$[dimOHmIm]^+,I^-$ and $[dimOHmBim]^+,I^-$ were investigated as a corrosion inhibitors for MS in 0.5 M H_2SO_4 using gravimetric, PDP and EIS techniques. Polarization curves revealed that both compounds acted as mixed-type inhibitors, and that corrosion IE% increased with their higher concentrations. The adsorption of both inhibitors onto the MS surface obeyed Langmuir's isotherm. The compound II showed a higher corrosion IE% than that of I. The quantum chemical calculations were applied to investigate the relationship between the two azolium salts derivatives electronic properties and their corrosion IE%.

Keywords: imidazolium and benzimidazolium salts, MS, polarization, EIS, WL and corrosion inhibition.

Introduction•

The prevention of metallic corrosion phenomena is vital, and must be accomplished with inorganic or organic inhibitors. However, the usage of some of them has been restricted, due to their toxicity and insufficient IE%, at low dosages [1-6]. The efficiency of corrosion inhibitors depends on environmental conditions, and on their interaction with metal surfaces, which is related with their structure, including their number of adsorption active centers, charge density and molecules size [7, 8].

• The abbreviations and symbols definition list are in pages 95-97.

MS enjoys wide application in industries, due its superior mechanical and physical characteristics. However, it is prone to quick corrosion in most service environments. Small amounts of inhibitor molecules may increase MS resistance to corrosive solutions, when they adsorb onto the metal surface and form a barrier that inhibits its active sites. The inhibitor molecular structure, different MSs and electrolytes have an impact on its adsorption [9-11].

Among the alternative corrosion inhibitors, organic compounds have been reported to effectively control MS dissolution in acidic media, especially those containing: N, O, P and S atoms; π bonds; and functional groups, such as NH-, -C = N-, -CHO and R-OH [12,13]. N-heterocyclic compounds, which are the most synthesized ones, are known to be excellent inhibitors for metallic corrosion [14, 15]. Recently, more studies have shown that IE% against MS corrosion in acidic solutions is enhanced by several organic compounds containing N [16]. It was shown that such compounds have protective properties that depend upon their ability to reduce W values, and that they are enhanced at higher electron densities around the N atoms [17-19].

On the other hand, it has been reported that ionic salts, with positively charged N^+, are important corrosion inhibitors in HCl and H_2SO_4. The effect of concentrations, functional groups and halide ions on Fe and steel corrosion has been extensively studied. The synergistic effect between organic cations and halide anions is considered to be an important factor in their inhibiting action on metallic corrosion [20-22].

Particular attention has been devoted to quaternary imidazolium salts that possess unique physical properties and chemical reactivity. From a chemical point of view, imidazolium and benzimidazolium derivatives can be considered as ionic N-heterocyclic salts. So, it has been considered of interest to investigate the inhibitory effect of these compounds on metallic corrosion.

The main objective of this work was the synthesis and IE% evaluation of the two azolium salts on MS corrosion in a 0.5 M H_2SO_4 medium. We incorporated other groups in the inhibitors structures, such as aromatic rings, and the hydroxyl function. We expected to obtain a wider surface adsorption and an excellent corrosion inhibitor. To further understand the corrosion IE%, theoretical investigations were made, and the temperature effect was studied. WL experiments, PDP measurements, EIS techniques and quantum chemical calculations were carried out in this work.

Experimental

Solutions

The aggressive solutions of 0.5 M H_2SO_4 were prepared by dilution of analytical grade 98% with distilled water. The concentration range of the employed inhibitors was from 0.1 to 5 mM (0.1 to 5 mmol/L).

Inhibitors

Compounds I and II were synthesized (Fig. 1), by treating one equivalent each of (1-methyl-1H-imidazol-2-yl)methanol and (1-methyl-1H-benzimidazol-2-yl)methanol, respectively, with 3 equivalents of methyl iodide in refluxing CH_3CN. The white solids

were filtered off, and then washed with CH_3CN. Suitable crystals of the compounds I and II were obtained through aqueous and CH_3CN/MeOH solutions evaporation, respectively. The X-ray crystallographic analysis of I and II single crystals confirmed their structures (Fig. 2).

I II

Figure 1. Inhibitors I and II chemical molecular structure.

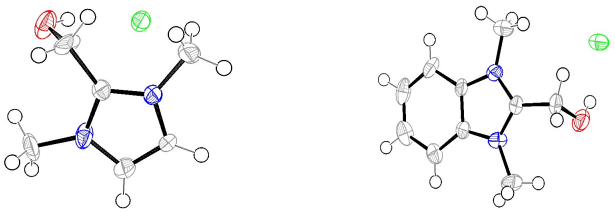

Figure 2. ORTEP plots of the X-ray crystal structures of inhibitors I and II. Displacement ellipsoids were drawn at 50% probability level. [23, 24].

WL experiments

WL experiments were performed on MS samples with the percentage composition of: 0.001 C; 0.242 Si; 0.628 Mn; 0.354 Na; 0.182 Al; 1.339 Cr; 0.149 Mo and Fe balance. The samples, with a rectangular shape of 13 × 10 × 0.5 mm, were represented in weight percentage (wt.%). Prior to the measurements, they were abraded by a series of emery papers (grades 120, 400 and 2000), washed with distilled water, degreased with ethanol, and finally dried at room temperature. After being accurately weighed by an analytical balance with a sensitivity of ±0.1 mg, the MS samples were immersed in a beaker containing 25 mL of an acidic solution, without and with inhibitors, at different concentrations. The temperature was controlled, at 298 K, by a water thermostat. The aggressive solutions were exposed to air. After immersion for 4 h, the corrosion products were completely removed. The samples were rinsed with distilled water, dried, and then re-weighed, in order to determine WL. W and IE% values were calculated according to the following equations:

$$W = \frac{\Delta m}{St} \quad (1)$$

$$IE(\%) = \frac{W_0 - W}{W_0} \quad (2)$$

where Δm (mg) is the weight loss, S (cm^2) is the area, t (h) is the immersion period, and W_0 ($mg/cm^{-2}/h^{-1}$) and W ($mg/cm^{-2}/Vh^{-1}$) are the MS corrosion rates, without and with inhibitors, respectively.

Electrochemical measurements

The electrochemical measurements were carried out in a conventional three-electrode cylindrical glass cell. The WE, in the form of a disc cut from MS, had a

geometric area of 1 cm^2. A SC and Pt were used as RE and AE, respectively. The temperature was thermostatically controlled at 298 K. Before measurements, the WE was mechanically polished, degreased with ethanol, rinsed several times with distilled water and dried. The freshly polished electrode was immersed in the test solution, at natural E, for 30 min, until a steady state was reached.
PPD and EIS measurements were performed using a ZRA GAMRY-reference 3000 potentiostat/galvanostat, at a scan rate of 1 mV/s^{-1}, in the E range from -800 to -200 mV. The IE% was determined from the following equation:

$$IE(\%) = \frac{I_{corr(0)} - I_{corr(inh)}}{I_{corr(0)}} \times 100 \quad (3)$$

where $I_{corr(0)}$ and $I_{corr(inh)}$ are the corrosion current densities, with and without inhibitors, respectively, which were determined by the extrapolation of anodic and cathodic Tafel lines to E_{corr}. Before all impedance measurements, the WE was immersed for 1 h in the acidic solution. EIS was performed at OCP, over a frequency range from 10 kHz to 10 mHz, with a 10 mV peak-to-peak amplitude, using the AC signal. The IE% for both inhibitors was calculated using the following equation:

$$IE(\%) = \frac{R_{ct(inh)} - R_{ct(0)}}{R_{ct(inh)}} \times 100 \quad (4)$$

where $R_{ct(0)}$ and $R_{ct(inh)}$ are the charge transfer resistance without and with inhibitors, respectively.

Computational studies

The two molecular geometries were fully optimized in the acidic solution, at the DFT level of theory. Theoretical calculations were performed using the ADF 2014.02 program package [25]. Electron correlation was treated within the VWN parametrization [26]. The hybrid type B3LYP functional was used for all calculations [27, 28]. The atomic electronic configurations were described by a triple-ζ STO basis set for H 1s, C 2s and 2p, N 2s and 2p, and O 2s and 2p, augmented with a 3d single-ζ polarization for C, N and O atoms, and with a 2p single-ζ polarization for H atoms. The vibrational frequency calculations were performed on all the optimized geometries, so as to verify that these structures corresponded to true minima on the MS surface E energy [29, 30].
The solvent effect, using COSMO-RS, which was developed by Klamt and co-workers [31], was studied. Representations of the orbitals and molecular structures were done using the ADF GUI [25]. To compare the chemical reactivity of inhibitors I and II, some quantum chemical parameters were calculated, such as: HOMO; LUMO; ΔE; μ; χ; IP; η; σ ; and ΔN from the inhibitors to the metal surface [32].

Results and discussion

WL

The effect of the tested inhibitors, with different concentrations, in 0.5 M H_2SO_4, on MS corrosion was studied by WL, at 298 K, after 4 h of immersion. The corresponding MS W and IE% values are shown in Table 1.

Table 1. MS WL data and corresponding IE%, in different concentrations of compounds I and II, at 298 K.

Inhibitors	C_{inh} (mM)	*W* (mg/cm^{-2}/ h^{-1})	*IE* %
Blank	0	1.15	-
Inhibitor I	0.1	0.87	24.34
	0.2	0.81	29.54
	0.5	0.67	41.73
	1	0.50	56.52
	2	0.45	60.86
	5	0.29	74.78
Inhibitor II	0.1	0.87	24.34
	0.2	0.85	26.08
	0.5	0.58	49.56
	1	0.52	54.78
	2	0.25	78.26
	5	0.18	84.34

As shown in Table 1, in an uninhibited solution, W value was 1.15 mg/cm^{-2}/h^{-1}. However, after adding compounds I and II, W values were greatly decreased with an increase in both inhibitors concentration, from 0.1 to 5 mM. Consequently, the inhibitors adsorption onto the MS surface, and its coverage, also increased, which enhanced their IE%. [33]. The maximum and minimum IE% values for inhibitor II were estimated to be 84.34 and 24.34%, at concentrations of 5 and 0.1 mM, respectively. On its turn, the compound I exhibited IE% values of 74.78 and 24.34%, at 5 and 0.1 mM concentrations, respectively. Therefore, both compounds I and II inhibited MS corrosion in 0.5 M H_2SO_4. However, compound II was found to be slightly more effective than I, probably because it had the benzene ring that encouraged a stronger interaction between it and the metal, resulting in its better adsorption.

OCP

Fig. 3 shows OCP evolution, as a function of time, for the solutions without and with compounds I and II, at the concentration of 5 mM.

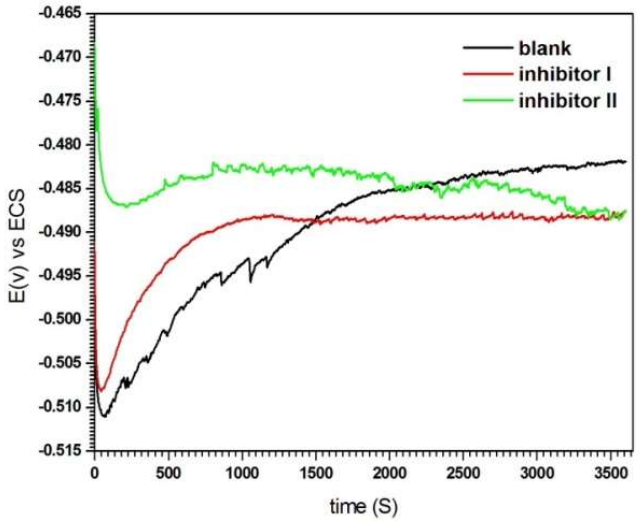

Figure 3. OCP of MS immersed in 0.5 M H_2SO_4 with and without inhibitors I and II.

In the solutions with inhibitors, the steady state was achieved in about 10 min, while in the blank solution it was achieved in approxim. 30 min. The electrode E finally became stable, which suggests the accomplishment of the steady state, where a dynamic equilibrium exists between the corrosion product deposition on the MS surface and its dissolution. It should be noted that OCP has shifted to more negative values in the inhibitors presence (-488 mV vs. SC electrode).

Polarization curves measurements

MS anodic and cathodic polarization behavior with and without inhibitors I and II, in 0.5 M H_2SO_4, at 298 K, for 30 min, is shown in Fig. 4. Various corrosion parameters, such as I_{corr}, E_{corr}, β_a, β_c and IE%, are given in Table 2.

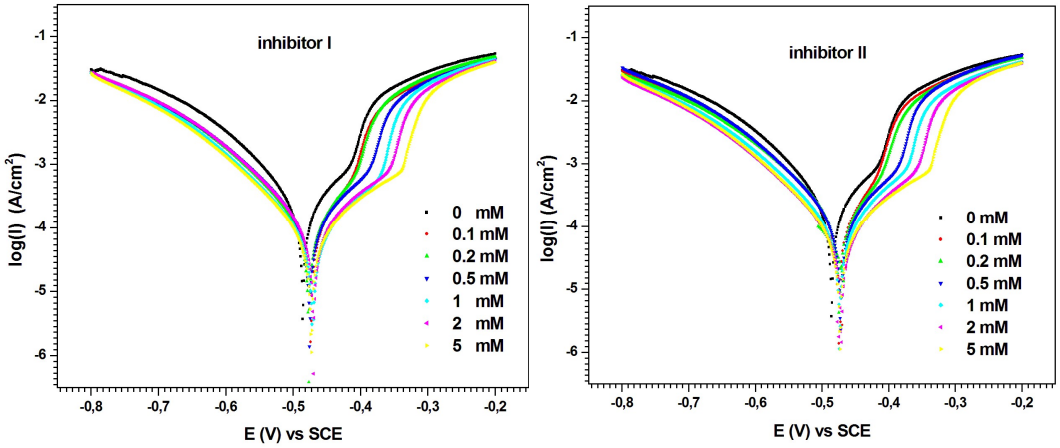

Figure 4. PDP curves for MS in 0.5 M H_2SO_4 with different concentrations of I and II.

Table 2 shows that I_{corr} decreased with increased concentrations of compounds I and II. Its lower value was obtained at 5 mM of both inhibitors.

Table 2. Studied MS electrochimical parameters at various concentrations of inhibitors I and II, in 0.5 M H_2SO_4, at 298 K.

	C_{inh} (mM)	E_{corr} (mV)	I_{corr} (µA/cm^{-2})	β_a (mV./dec^{-1})	β_c (mV/ dec^{-1})	IE (%)
Blank	0	-485	362	119.2	144.2	-
Inhibitor I	0.1	-474	185	104.3	140.8	49.17
	0.2	-477	177	104.0	138.7	51.10
	0.5	-475	161	104.6	135.6	55.52
	1	-471	84.3	93.9	122.4	76.71
	2	-472	81.3	99.9	122.0	77.54
	5	-473	78.7	108	121.1	78.25
Inhibitor II	0.1	-475	240	107.6	145.8	33.70
	0.2	-474	229	107.5	147.0	36.74
	0.5	-472	170	101.1	133.2	53.03
	1	-474	117	99.8	130.4	67.68
	2	-472	104	100.5	125.8	71.27
	5	-472	76.7	108.0	121.1	78.81

Consequently, the compounds IE% increased with their higher concentrations, which was due to their stronger adsorption onto the corroded MS surface [34].

On the other hand, according to the polarization curves (Fig. 4), the higher concentrations of inhibitors I and II promoted a decrease in both anodic and cathodic I_{corr}, with a slight E_{corr} shift towards the anodic direction. These results show that the inhibitors addition slowed MS half-cells corrosion reactions. However, their impact was more pronounced on the anodic reactions [35, 36]. In other words, the studied compounds I and II can be classified as mixed-type inhibitors, with a major control over the metal dissolution anodic reaction.
As seen in Table 2, PDP measurements show that both inhibitors achieved practically the same IE%, at a concentration of 5 mM. However, at lower concentrations (0.1 to 2 mM), compound I was a better corrosion inhibitor than II. For example, at the lowest concentration (0.1 mM), compound I showed an IE above 49.17%, whereas that of compound II was below 33.7%.

EIS

Fig. 5 shows the Nyquist diagrams for MS in 0.5 M H_2SO_4, without and with compounds I and II, at different concentrations. The electrochemical parameters derived from the Nyquist diagrams are given in Table 3.

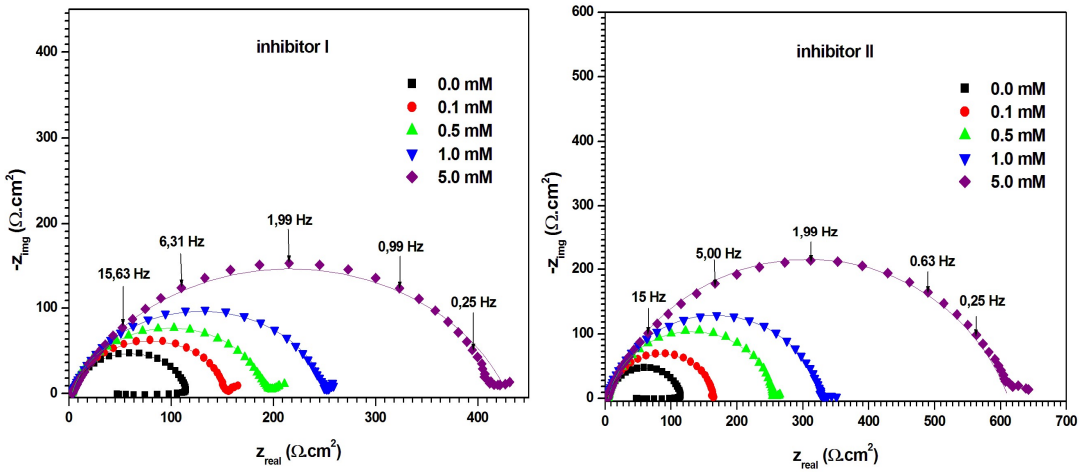

Figure 5. Nyquist diagrams for MS in 0.5 M H_2SO_4, without and with inhibitors I and II, in different concentrations, at 298 K (solid lines show fitted results).

Fig. 5 shows that the Nyquist diagram obtained for the blank solution consists of a capacitive loop, with a large diameter at high frequencies (related to the C_{dl} behavior, and R_{ct} of the corrosion process), followed by a small inductive loop at a low frequency. As mentioned by Hsu and Mansfeld [37], the low frequency inductive loop may be the result of the relaxation process obtained by $FeSO_4$ adsorption onto the electrode surface. It might be also attributed to the passivated surface re-dissolution at low frequencies [38].
On the other hand, Nyquist diagrams, for inhibitors I and II in H_2SO_4, contain a capacitive loop at high frequency values, followed by a straight line at low frequencies. The high frequency capacitive loop is related to the corrosion process R_{ct}. The low frequency straight line implies that MS corrosion in the 0.5 M H_2SO_4 solution was diffusion controlled [39]. Clearly, the capacitive loops in the solutions

with inhibitors were larger than in those without them, and increased progressively with higher concentrations of compounds I and II. Furthermore, the capacitive loops diameters were larger with inhibitor II than with I.
In Fig. 6, CPE [40] was introduced into the circuit, instead of a pure C_{dl}, in order to give a more accurate fit [41]. This impedance element was calculated by the following equation [41]:

$$Z_{CPE} = [Y_0 \times (j\omega)^n]^{-1} \quad (5)$$

where Y_0 is the constant, j is the imaginary number ($j^2 = -1$), ω is the angular frequency and n is the coefficient. C_{dl} can be calculated using the following equation [42]:

$$C_{dI} = (Y_0 \times R_{ct}{}^{(1-n)})^{1/n} \quad (6)$$

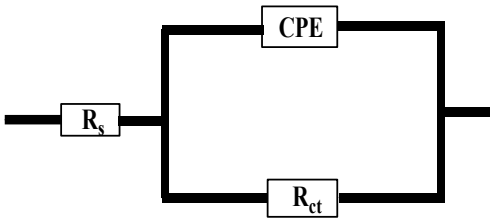

Figure 6. Equivalent circuit diagram used to fit impedance data.

Table 3 shows that R_{ct} increased, while C_{dl} decreased, at higher inhibitors concentrations.

Table 3. Impedance measurements and IE% for MS corrosion in 0.5 M H_2SO_4 with various concentrations of inhibitors I and II, at 298 K.

	C_{inh} (mM)	R_s ($\Omega.cm^2$)	R_{ct} ($\Omega.cm^2$)	n	Y_0 ($S^n.cm^{-2}.\Omega^-$)	C_{dl} ($\mu F.cm^{-2}$)	EI %
Blank	0	3.481	113.8	0.8779	546	371	-
Inhibitor I	0.1	3.388	154.3	0.8581	422	268	26.2
	0.5	3.272	194.9	0.8595	381	248	41.6
	1	3.76	251.1	0.836	316	192	54.6
	5	3.357	424.8	0.7669	341	189	73.2
Inhibitor II	0.1	3.988	162.1	0.8955	316	223	29.7
	0.5	4.893	254.6	0.8719	260	174	55.3
	1	4.050	327.7	0.8543	230	147	65.2
	5	3.868	614.0	0.7842	213	121	81.4

The increase in R_{ct} may have been due to the formation of a protective film on the MS/H_2SO_4 interface. The higher C_{dl} value (371 μF/cm^{-2}) without inhibitor may indicate that the MS surface was fully covered with H^+. However, the decrease in C_{dl} values, with inhibitors, can be attributed to the increase in the electrical double layer thickness and/or to a reduction in the local dielectric constant, indicating that the inhibition mechanism functioned by adsorption onto the metal surface [43-45]. On the other hand, according to the Bode plots of the evaluated inhibitors (Fig. 7), Z_{mod} rose when their concentrations increased, which indicates better IE% [46].

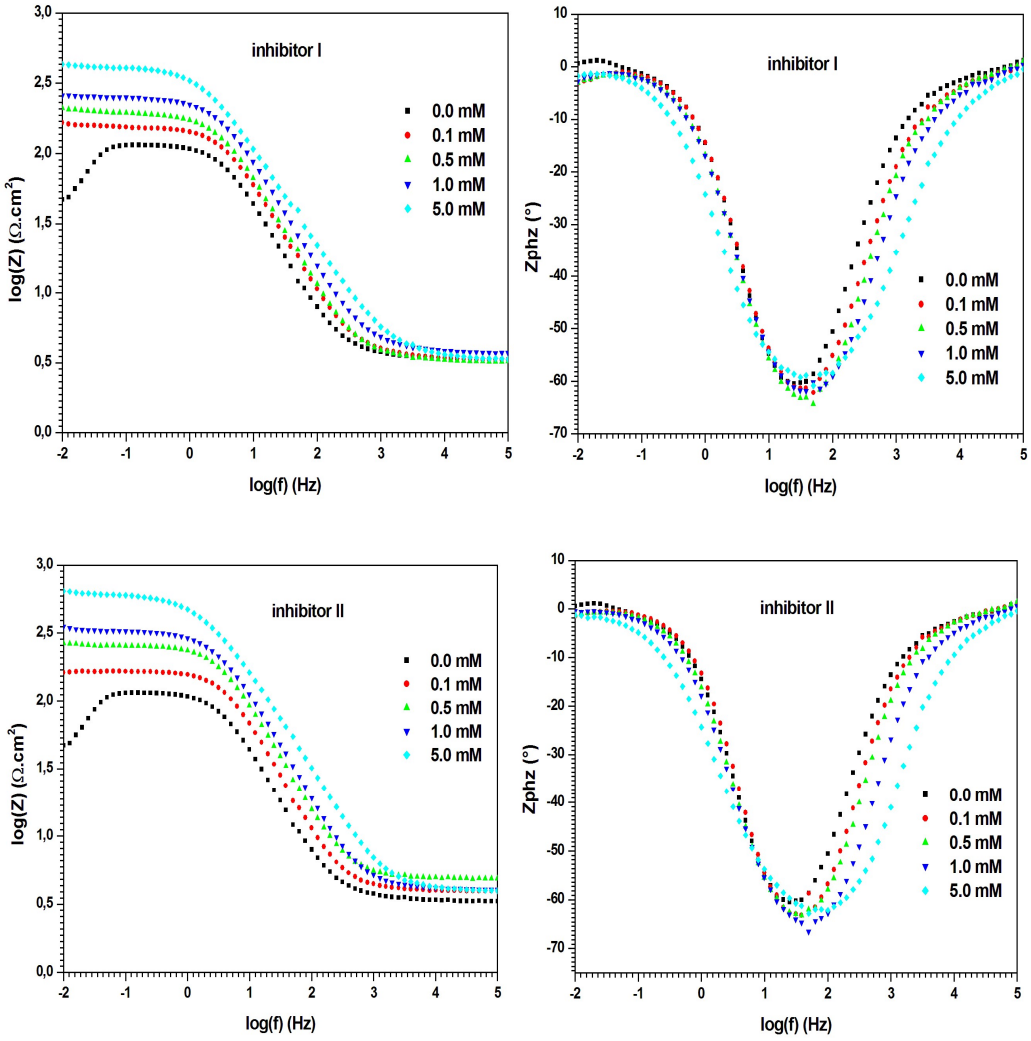

Figure 7. Bode plots of MS in 0.5 M H_2SO_4 without and with inhibitors I and II.

EIS recorded higher corrosion IE% for inhibitor II (81.4%) than that of I (73.2%), at their higher concentrations (5 mM), in 0.5 M H_2SO_4. These results are in good agreement with the ones obtained from PDP measurements.

Adsorption isotherms

The adsorption isotherms can give valuable information on the interaction between inhibitor and metal surface. In order to clarify the adsorption nature and strength, attempts were made to fit experimental data to various isotherms, including Frumkin's, Langmuir's and Temkin's.

Plots of C_{inh}/θ against C_{inh} (Fig. 8) gave a straight line with a correlation close to 1, for inhibitors I (r = 0.9994) and II (r = 0.99899), suggesting that their adsorption onto the MS surface obeyed Langmuir's adsorption isotherm, which can be expressed by the following equation [47]:

$$\frac{C_{inh}}{\theta} = \frac{1}{K} + C_{inh} \qquad (7)$$

where C_{inh} is the inhibitors concentrations and θ is the surface coverage, which was determined from Tafel plot.

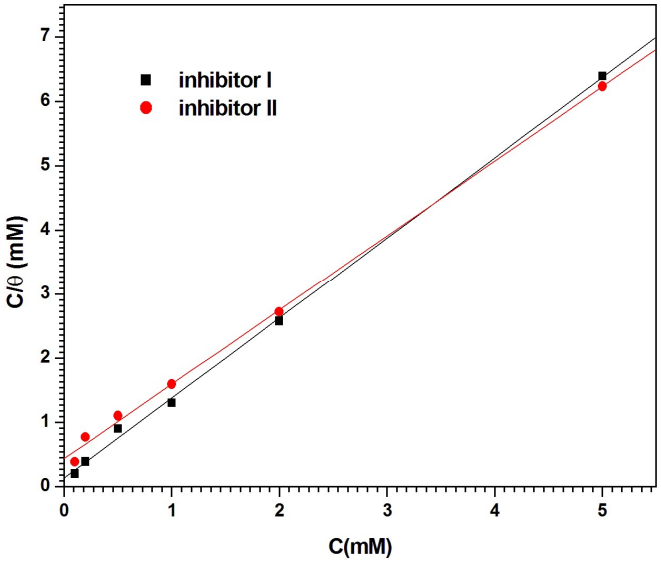

Figure 8. Langmuir's isotherm plots for the adsorption of inhibitors I and II onto the MS surface.

The K values were calculated from the straight lines intercepts with C_{inh}/θ axis, and are 7.604×10^3 and 2.295×10^3 M^{-1}, for inhibitors I and II, respectively. These values reflect the formation of stable adsorbed inhibitors layers, and their strong interaction with the metal surface.
ΔG^0_{ads}, onto the MS surface, is related to K in the following equation:

$$K = \frac{1}{55,5} \exp\left(\frac{-\Delta G^0_{ads}}{RT}\right) \quad (8)$$

where R is the universal gas constant, T is the absolute temperature and 55.5 is the water concentration in the solution, expressed in moles [48].
Literature shows that ΔG°_{ads} values: around -20 kJ/mol^{-1} or lower (more positive), indicate the inhibitor molecules electrostatic interaction with MS (physical adsorption) [49, 50]; and below -40 kJ/mol^{-1}, involve charge sharing between the inhibitor molecules and MS (chemisorption). Therefore, the calculated ΔG°_{ads} values (-32.1 and -29.1 kJ/mol^{-1}, for inhibitors I and II, respectively) indicate that the inhibitors adsorption onto the MS surface probably took place via both chemical and physical adsorptions.

Temperature effect on corrosion electrochemical parameters

The temperature effect on corrosion electrochemical parameters was determined from 298 to 328 K, without and with 1 mM of compounds I and II in 0.5 M H_2SO_4, using PDP measurements. E_a for MS corrosion in 0.5 M H_2SO_4 without and with 1.0 mM inhibitors was calculated using Arrhenius equation:

$$I_{corr} = k \exp\left(-\frac{E_a}{RT}\right) \quad (9)$$

where k is the Arrhenius pre exponential factor and R is the gas constant. According to the data in Table 4, the plots of $\ln(I_{corr})$ versus 1/T (Fig. 9) have almost straight lines, and all the r values are close to 1.

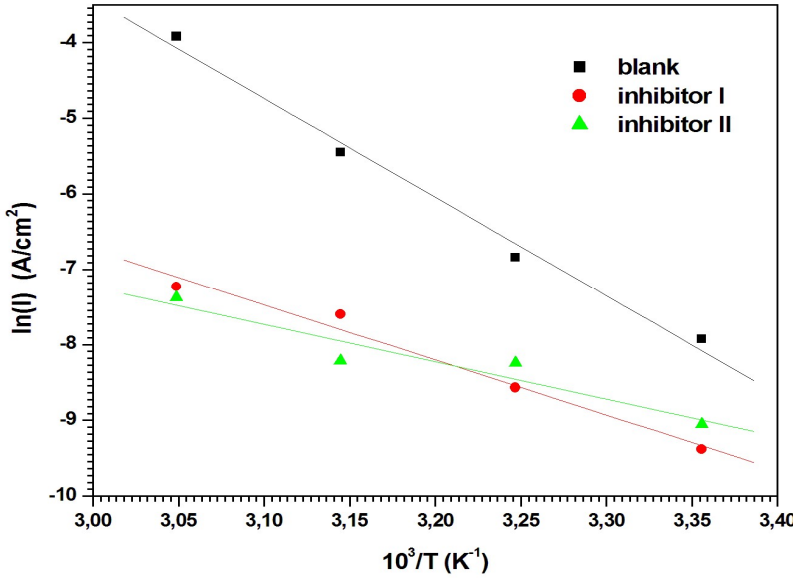

Figure 9. Arrhenius plots of ln(I) *vs* 10^3/T for MS corrosion in 0.5 M H_2SO_4 with inhibitors I and II.

Table 4 shows that E_a values, which were calculated from the slopes of the straight lines, were lower with inhibitors I and II than those without them. It is well recognized that the increase in the corrosion IE% with temperature corresponds to an apparently lower E_a value than that without inhibitors [51]. This demonstrates that both inhibitors were adsorbed onto the metal surface, forming strong chemisorption bonds [52]. The decrease in E_a value can be ascribed to the slow rate of the inhibitors adsorption onto the MS surface, with a resultant closer approach to equilibrium, during the experiments at higher temperatures [53].

Table 4. Temperature effect on corrosion electrochemical parameters in 0.5 M H_2SO_4, without and with inhibitors I and II, at a concentration of 1.0 Mm.

	T (K)	E_{corr} (mV)	I_{corr} (µA/cm^{-2})	*IE* %	E_a (kJ/mol)
Blank	298	-485	362	-	108
	308	-478	1072	-	
	318	-478	4300	-	
	328	-481	19900	-	
Inhibitor I	298	-471	84.3	76.79	60
	308	-478	190	82.27	
	318	-477	502	88.32	
	328	-477	724	96.36	
Inhibitor II	298	-474	117	67.67	41
	308	-479	268	75.00	
	318	-484	271	93.69	
	328	-479	625	96.85	

Computational studies

The quantum chemical parameters, such as E_{HOMO} and E_{LUMO}, ΔE and µ, have been determined for establishing possible relations between the structures of

compounds I and II and their IE% (Table 5). The inhibitors optimized structures, HOMO and LUMO are shown in Fig. 10.

Table 5. Inhibitors I and II quantum chemical parameters calculated at DFT level, using the hybrid /B3LYP/TZP basis set obtained in the aqueous solutions.

Inhibitors	Total energy (eV)	E_{HOMO} (eV)	E_{LUMO} (eV)	ΔE (eV)	μ (D)	A (eV)	I (eV)	η	σ	χ	ΔN
I	-129.716	-7.528	-1.409	6.119	20.944	1.409	7.528	3.059	0.326	4.468	0.716
II	-178.125	-7.167	-1.988	5.179	20.702	1.988	7.167	2.589	0.386	4.577	0.747

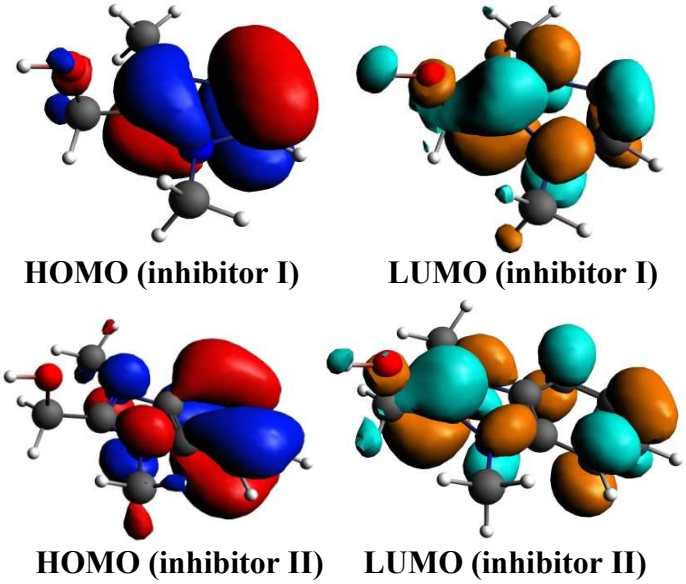

Figure 10. Inhibitors I and II HOMO and LUMO at the hybrid/B3LYP/TZP.

The inhibitor molecules adsorption onto the metal surface was due to interactions between the heterocyclic compound π-electrons and the MS surface atoms vacant d-orbital. Generally, E_{HOMO} is related to the molecules donation of electrons. Its high values indicate the inhibitors molecules strong donation of electrons to the appropriate acceptor, and also facilitate their adsorption (i.e. inhibition action). E_{LUMO} is related to the molecules acceptance of electrons. Lower the E_{LUMO} value, higher is the probability of the metal molecules to accept electrons from the inhibitors molecules. Also, higher ΔE values will provide low reactivity to a chemical species. On the contrary, its decreased values will render good IE%, because the energy to remove an electron from the LUMO will be low.

From Table 5, it is clear that inhibitor II has a higher E_{HOMO} value than that of I. This means that the electrons donating capacity of compound II was higher than that of I. This led to its stronger adsorption onto the MS surface, thus increasing its IE%. Also, the quantum chemical calculations confirm that inhibitor II had E_{LUMO} and ΔE lower values than those of I.

Furthermore, compound II had σ and E_{ea} higher values and η and IP lower values than those of I, which confirms its higher IE%, which is in good agreement with the experimental observations. Also, it is clear that the ΔN values of both

compounds were positive; therefore, electrons were transferred from both inhibitors to the metal atoms.

On the other hand, inhibitor II molecular surface area (imidazole is a part of benzimidazole) and weight higher values than those of I enhanced its effective coverage of the MS surface, leading to its stronger IE%.

The comparison obtained from the Mulliken charges, on the optimized structure of both inhibitors atoms, shows that the active adsorptive O atoms were more negative (Fig. 11). So, these atoms acted as donors of electrons, and there was an electrostatic attraction between the MS surface and both inhibitor molecules.

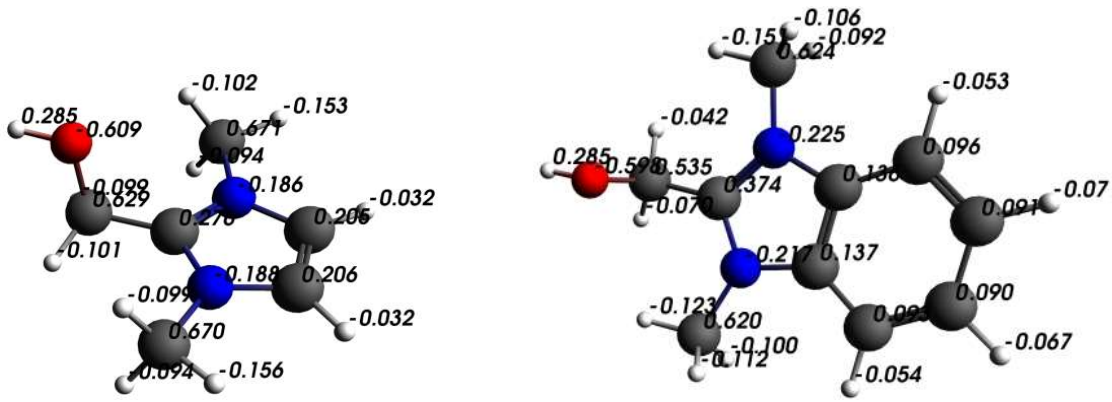

Inhibitor I **Inhibitor II**

Figure 11. Inhibitors I and II charge density, at the hybrid/B3LYP/TZP.

Explanation for the inhibition mechanism

At the electrochemical and gravimetric experiments completion, H_2SO_4 with inhibitors I and II became yellow colored, with elapsed time.

In order to explain the apparition of this color, and the compounds inhibition mechanism, a concentrated H_2SO_4 solution with inhibitor I was exposed to air, after the experiments. During this period, the transformation of $[dimOHmIm]^+$, I^- to/ I^-_3 ions occurred, producing a pronounced yellow color in the studied H_2SO_4 solution, and some crystals, which resulted from water evaporation. The crystals of the compound $[dimOHmIm]^+,I_3^-$ were isolated, and their structure was determined by an X-ray crystallographic analysis (Fig. 12).

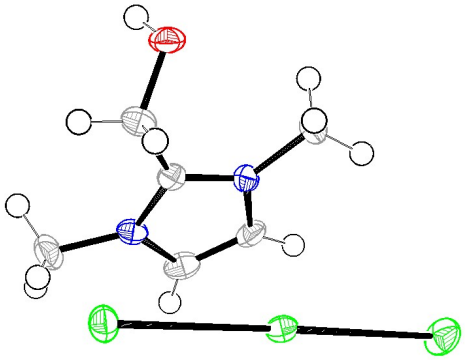

Figure 12. ORTEP plots of the X-ray crystal structure of $[dimOHmIm]^+$, I_3^- . Displacement ellipsoids were drawn at the 50% probability level [54].

The isolated compound $[dimOHmIm]^+ I_3^-$ asymmetric unit contains a 2-hydroxymethyl-1,3-dimethylimidazolium cation and a tri-iodide anion. This compound production is explained by the following equations:

$$[dimOHmIm]^+, I^- \longrightarrow [dimOHmIm]^+ + I^- \quad (10)$$

$$4I^- + O_2 + 4H^+ \longrightarrow 2I_2 + 2H_2O \quad (11)$$

$$I^- + I_2 \longrightarrow I_3^- \quad (12)$$

$$6I^- + O_2 + 4H^+ \longrightarrow 2\,I_3^- + 2H_2O \quad (13)$$

Compound I was ionized in the aqueous acidic solution, as shown in equation (10). Then, the iodide ion was oxidized by molecular O_2 dissolved in the H_2SO_4 solution, giving an equivalent of iodine that, in turn, formed 2 new moles of I_3^-, through the reaction shown in equation 11. Then, I_3^- exhibited a yellow color. The overall result of the electrochemical reactions (equations 10, 11 and 12) is expressed by equation 13 [55].

The $[dimOHmIm]^+$,I_3^- adsorption and inhibition effect in the H_2SO_4 solution can be explained as follows:

The I_3^- and/or I^- ions are soluble, and gradually cloud-accumulated near the MS/solution interface. After being adsorpted, they created an excess negative charge towards the solution, and favored the $[dimOHmIm]^+$ cation adsorption, through an electrostatic interaction with the negative charged MS surface.

In order to study the counter ion nature influence, and the time effect, on the IE% of compound I, PDP tests were performed using three electrolyte solutions with the inhibitor (5 mM): the first one was freshly prepared; and the second and third ones were aged for 48 and 72 h, respectively, at room temperature, before measurements.

As the solutions aged at room temperature, a yellow color, that characterizes the transformation of I^- to I_3^- ions, began to be pronounced. The three solutions IE% are presented in Fig. 13.

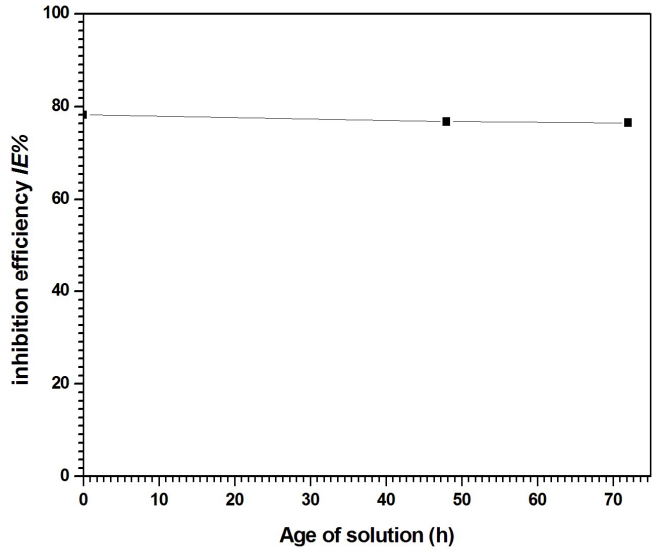

Figure 13. IE% variation of compound I with the solution ageing.

It is clear from Fig. 13 that, after 72 h, IE% did not significantly change (78.25 and 76.48%, for the freshly prepared and 72 h aged solutions, respectively). On the other hand, when $[dimOHmIm]^+$ was adsorbed onto the MS surface, an electron was transferred from the inhibitor polar atom (O and/or N) to the metal surface, forming a coordinate type of bond.
This result means that both physical and chemical adsorption took place, and that there was a combined action between the inorganic anions I^- and/or I_3^- and the organic cation $[dimOHmIm]^+$.
Concerning the inhibitor II mechanism, we suggest that it may be the same from that of compound I.

Conclusion

The tested compounds can be effectively used as corrosion inhibitors for MS in H_2SO_4. The order of the compounds I and II IE%, as given by polarization measurements, is in good agreement with that obtained from EIS measurements and WL. Both inhibitors IE% increased with their higher concentrations. Potentiostatic polarization data indicated that these compounds influenced both cathodic and anodic processes, which means that they are mixed-type inhibitors. The compounds adsorption onto the MS surface obeyed Langmuir's isotherm, and probably took place via both chemical and physical mechanisms. Quantum chemical calculations were carried out to compare the two inhibitors IE%. The results obtained from all the experimental methods were in good agreement.

Authors' contributions

Mohamed Elhadi Said: conceived and designed the analysis; collected the data; inserted data or analysis tools; performed the analysis; wrote the paper. **Mehdi Bouchouit**: inserted data or analysis tools. **Abdellah Zaiter**: conceived and designed the analysis; inserted data or analysis tools; wrote the paper. **Bilel Mezhoud**: conceived and designed the analysis; performed the analysis. **Sofiane Bouacida**: conceived and designed the analysis; collected the data; wrote the paper. **Aissa Chibani**: conceived and designed the analysis; inserted data or analysis tools; wrote the paper. **Abdelmalek Bouraiou**: performed the analysis; wrote the paper.

Abbreviations

AC: alternating current
ADF: Amsterdam density functional
AE: auxiliary electrode
-C = N-: imine
C_{dl}: double layer capacitance
CH_3CN: acetonitrile
-CHO: aldeyde
Compound I: **[**$dimOHmIm]^+$,I^-
Compound II: $[dimOHmBim]^+$,I^-
COSMO-RS: conductor-like screening model for realistic solvent
CPE: constant phase element

[dimOHmBim]$^{+}$,I^{-}: 1,3-dimethyl-2-hydroxymethylbenzimidazolium iodide inorganic anion
[dimOHmIm]$^{+}$: 1,3-dimethyl-2-hydroxymethylimidazolium organic cation
[dimOHmIm]$^{+}$,I^{-}: 1,3-dimethyl-2-hydroxymethylimidazolium iodide inorganic anion
[dimOHmIm]$^{+}$, I_3^-: 1,3-dimethyl-2-hydroxymethylimidazolium containing an organic cation and a triiodide inorganic anion
D: Debye
E: potential
E_a: activation energy
E_{corr}: corrosion potential
E_{ea}: electron affinity
E_{HOMO}: energy of the highest occupied molecular orbital
EIS: electrochemical impedance spectroscopy
E_{LUMO}: energy of the lowest occupied molecular orbital
$FeSO_4$: ferrous sulfate
GUI: graphical user interface
H_2SO_4: sulphuric acid
HCl: hydrochloric acid
HOMO: highest occupied molecular orbital
I_{corr}: corrosion current density
IE%: inhibition efficiency
IP: ionization potential
K: adsorption equilibrium constant
LUMO: lowest unoccupied molecular orbital
MeOH: methanol
MS: mild steel
-NH-: amine
OCP: open circuit potential
PDP: potentiodynamic polarization
r: correlation coefficient
RE: reference electrode
R_{ct}: charge transfer resistance
R-OH: alcohol
R_s: solution resistance
SC: saturated calomel
SEM: scanning electron microscopy
STO: slater-type orbital
VWN: Vosko−Wilk−Nusair
W: corrosion rate
WE: working electrode
WL: weight loss
Z_{mod}: peaking off impedance mode

Symbols definitions:
β_a: anodic Tafel slope
β_c: cathodic Tafel slope

ΔE: gap energy
ΔG°_{ads}: standard free energy of adsorption
ΔN: fraction of electrons transferred
μ: dipole moment
η: hardness
μF: microfarad
σ: softness
χ: electronegativity

References

1. Perez N. Electrochemistry and Corrosion Science, Kluwer Academic Publishers Boston. 2004.
2. Traibanelli G. Corrosion. 1991;47:410-419. https://doi.org/10.5006/1.3585271
3. Deng S, Li X, Fu H. Alizarin violet 3B as a novel corrosion inhibitor for steel in HCl, H_2SO_4 solutions. Corros Sci. 2011;53:3596-3602. https://doi.org/10.1016/j.corsci.2011.07.003
4. Bouklah M, Ouassini A, Hammouti B et al. Corrosion inhibition of steel in 0.5 M H_2SO_4 by [(2-pyridin-4-ylethyl)thio]acetic acid. Appl Surf Sci 2005;250:50-56. https://doi.org/10.1016/j.apsusc.2004.12.021
5. Abdelaziz S, Benamira M, Messaadia L et al. Green corrosion inhibition of mild steel in HCl medium using leaves extract of *Arbutus unedo* l. plant: An experimental and computational approach. Coll Surf A: Physicochem Eng Asp. 2021;619;126496-126509. https://doi.org/10.1016/j.colsurfa.2021.126496
6. Singh P, Chauhan DS, Chauhan SS et al. Synergistic Effect of Iodide Ion and N-methyl-N,N,N- trioctylammonium Chloride on Corrosion Inhibition of Carbon Steel in 0.5 M H_2SO_4: Experimental and Computational Approach. Chem Select. 2021;6:11417-11430. https://doi.org/10.1002/slct.202102837
7. Kadhim A, Betti N, Al-Bahrani HA et al. A mini review on corrosion, inhibitors and mechanism types of mild steel inhibition in an acidic environment. Int J Corros Scale Inhib. 2021;10(3):861-884. https://doi.org/10.17675/2305-6894-2021-10-3-2
8. Cao Z, Tang Y, Cang H et al. Novel benzimidazole derivatives as corrosion inhibitors of mild steel in the acidic media. Part II: Theoretical studies. Corros. 2014;83:292-298. https://doi.org/10.1016/j.corsci.2014.02.025
9. Edoziuno FO, Adediran AA, Odoni BU et al. Influence of wormin mebendazole on the corrosion of mild steel in 1.0 M sulphuric acid. Results in Eng. 2021;9:100192. https://doi.org/10.1016/j.rineng.2020.100192
10. Zheng X, Zhang S, Li W et al. Investigation of 1-butyl-3-methyl-1*H*-benzimidazolium iodide as inhibitor for mild steel in sulfuric acid solution. Corros Sci. 2014;80:383-392. https://doi.org/10.1016/j.corsci.2013.11.053
11. Kumar H, Dhanda T. 5-Aminotetrazole a highly efficient corrosion inhibitor for mild steel in 0.1 N sulphuric acid: Experimental and theoretical study. Chem Data Collect. 2021;33:100721. https://doi.org/10.1016/j.cdc.2021.100721
12. Oguzie EE. Corrosion inhibition of mild steel in hydrochloric acid solution by methylene blue dye. Mat Lett. 2004;59:1076-1079. https://doi.org/10.1016/j.matlet.2004.12.009

13. Li X, Deng S, Fu H et al. Inhibition effect of 6-benzylaminopurine on the corrosion of cold rolled steel in H_2SO_4 solution. Corros Sci.2008;51:620-634. https://doi.org/10.1016/j.corsci.2008.12.021
14. Elayyachy M, Elkodadi M, Aouniti A et al. New bipyrazole derivatives as corrosion inhibitors for steel in hydrochloric acid solutions. Mater Chem Phys. 2005;93:281-285. https://doi.org/10.1016/j.matchemphys.2005.03.059
15. Muralidharan S, Quraishi MA, Iyer SVK. The effect of molecular structure on hydrogen permeation and the corrosion inhibition of mild steel in acidic solutions. Corros Sci. 1995;37:1739-1750 https://doi.org/10.1016/0010-938X(95)00068-U
16. Boughoues Y, Benamira M, Messaadia L. Experimental and theoretical investigations of four amine derivatives as effective corrosion inhibitors for mild steel in HCl medium. RSC Adv. 2020;10:24145-24158. https://doi.org/10.1039/d0ra03560b
17. Quraishi MA, Ahmad S, Ansari MQ. Inhibition of steel corrosion by some new triazole derivatives in boiling hydrochloric acid. Br Corros J. 1997;32:297-300. https://doi.org/10.1179/000705997798129223
18. Bentiss F, Lagrenee M, Traisnel M, et al. The Corrosion Inhibition of Mild Steel in Acidic Media by a New Triazole Derivative. Corros Sci. 1999;41:789-803. https://doi.org/10.1016/S0010-938X(98)00153-X
19. Chetouani A, Hammouti B, Benhadda T et al. Inhibitive action of bipyrazolic type organic compounds towards corrosion of pure iron in acidic media. Appl Surf Sci. 2005;249:375-385. https://doi.org/10.1016/j.apsusc.2004.12.034
20. Frignani A, Zucchi F, Monticelli C. Inhibition of iron corrosion in different acid media by N-Decyl-Pyridinium derivatives. Br Corros J. 1983;18:19-24. https://doi.org/10.1179/000705983798274029
21. Schweinsberg DP, Ashworth V. The inhibition of the corrosion of pure iron in 0.5 M sulphuric acid by n-alkyl quaternary ammonium iodides. Corros Sci. 1988;28:539-545. https://doi.org/10.1016/0010-938X(88)90022-4
22. Niu L, Zhang H, Wie F et al. Corrosion inhibition of iron in acidic solutions by alkyl quaternary ammonium halides: Correlation between inhibition efficiency and molecular structure. Appl Surf Sci. 2005;252:1634. https://doi.org/10.1016/j.apsusc.2005.02.134
23. Said M El H, Bouacida S, Merazig H et al. 2-Hydroxymethyl-1,3-dimethy l-1H-benzimidazol-3-ium iodide. Acta Crystallogr. 2013;69:429-1430. https://doi.org/10.1107/S1600536813022307
24. Cambridge Crystallographic Data Centre: supplementary publication numbers CCDC 950210 for I. This data can be obtained free of charge from The Cambridge Crystallographic Data Centre via www.ccdc.cam.ac.uk/data_request/cif./cif
25. ADF2014.02; SCM, Theoretical Chemistry, Vrije Universiteit: Amsterdam, The Netherlands. https://www.scm.com

26. Vosko SD, Wilk L, Nusair M. Accurate spin-dependent electron liquid correlation energies for local spin density calculations: a critical analysis. Can J Chem. 1980;58:1200-1211. https://doi.org/10.1139/p80-159
27. Becke AD. Density-functional exchange-energy approximation with correct asymptotic behavior. Phys Rev A. 1988(6);38:3098-3100. https://doi.org/10.1103/PhysRevA.38.3098
28. Perdew JP. Density-functional approximation for the correlation energy of the inhomogeneous electron gas. Phys Rev B. 1986;33:8822-8824. https://doi.org/10.1103/PhysRevB.33.8822
29. Fan L, Ziegler T. Application of density functional theory to infrared absorption intensity calculations on main group molecules. J Chem Phys. 1992;96(12):9005-9012. https://doi.org/10.1063/1.462258
30. Fan L, Ziegler T. Application of density functional theory to infrared absorption intensity calculations on transition-metal carbonyls. J Phys Chem. 1992;96(17):6937-6941. https://doi.org/10.1021/j100196a016
31. Klamt A, Schüümann G. COSMO: a new approach to dielectric screening in solvents with explicit expressions for the screening energy and its gradient. J Chem Soc Perkin Trans. 1993;2:799-805. https://doi.org/10.1039/P29930000799
32. Nyijime TA, Ayuba AM. Quantum Chemical Studies and Molecular Modeling of the Effect of *Coriandrum Sativum L.* Compounds as Corrosion Inhibitors on Aluminum Surface. Appl J Envir Eng Sci. 2020;6(4);344-355. https://doi.org/10.48422/IMIST.PRSM/ajees-v6i4.22958
33. Li X, Mu G. Tween-40 as corrosion inhibitor for cold rolled steel in sulphuric acid: weight loss study, electrochemical characterization, and AFM. Appl Surf Sci. 2005;252:1254-1265. DOI:https://doi.org/10.1016/j.apsusc.2005.02.118
34. Safak S, Duran B, Yurt A et al. Schiff bases as corrosion inhibitor for aluminium in HCl solution. Corros Sci. 2012;54:251-259. https://doi.org/10.1016/j.corsci.2011.09.026
35. Finšgar M, Lesae A, Kokalj A et al. A comparative electrochemical and quantum chemical calculation study of BTAH and BTAOH as copper corrosion inhibitors in near neutral chloride solution. Electrochim Acta. 2008;53:8287-8297. https://doi.org/10.1016/j.electacta.2008.06.061
36. Lebrini M, Lagrenée M, Traisnel M et al. Enhanced corrosion resistance of mild steel in normal sulfuric acid medium by 2,5-bis(n-thienyl)-1,3,4-thiadiazoles: Electrochemical, X-ray photoelectron spectroscopy and theoretical studies. Appl Surf Sci. 2007;253:9267-9276. https://doi.org/10.1016/j.apsusc.2007.05.062
37. Hsu CH, Mansfeld F. Technical Note: Concerning the Conversion of the Constant Phase Element Parameter Y_0 into a Capacitance. Corrosion. 2001;57:747-748. https://doi.org/10.5006/1.3280607
38. Singh AK, Quraishi MA. Effect of Cefazolin on the corrosion of mild steel in HCl solution. Corros Sci. 2010;52:152-160. https://doi.org/10.1016/j.corsci.2009.08.050
39. Solmaz R, Altunbaş Şahin E, Döner A et al. The investigation of synergistic inhibition effect of rhodanine and iodide ion on the corrosion of copper in sulphuric acid solution. Corros Sci. 2011;53:3231-3240. https://doi.org/10.1016/j.corsci.2011.05.067

40. Ma H, Cheng X, Li G et al. The influence of hydrogen sulfide on corrosion of iron under different conditions. Corros Sci. 2000;42:1669-1683. https://doi.org/10.1016/S0010-938X(00)00003-2
41. Benedeti AV, Sumodjo PTA, Nobe K et al. Electrochemical studies of copper, copper-aluminium and copper-aluminium-silver alloys: Impedance results in 0.5 M NaCl. Electrochim Acta. 1995;40:2657-2668. https://doi.org/10.1016/0013-4686(95)00108-Q
42. Azghandi MV, Davoodi A, Farzi GA et al. Water-base acrylic terpolymer as a corrosion inhibitor for SAE1018 in simulated sour petroleum solution in stagnant and hydrodynamic conditions. Corros Sci. 2012;64:44-54. https://doi.org/10.1016/j.corsci.2012.07.003
43. Prabhu RA, Venkatesha TV, Shanbhag AV et al. Inhibition effects of some Schiff's bases on the corrosion of mild steel in hydrochloric acid solution. Corros Sci. 2008;50:3356-3362. https://doi.org/10.1016/j.corsci.2008.09.009
44. Tang Y, Yang X, Yang W et al. Experimental and molecular dynamics studies on corrosion inhibition of mild steel by 2-amino-5-phenyl-1, 3, 4-thiadiazole. Corros Sci. 2010;52:242-249. https://doi.org/10.1016/j.corsci.2009.09.010
45. Goulart CM, Esteves-Souza A, Martinez-Huitle CA et al. Experimental and theoretical evaluation of semicarbazones and thiosemicarbazones as organic corrosion inhibitors. Corros Sci. 2013;67:281-291. https://doi.org/10.1016/j.corsci.2012.10.029
46. Hegazy MA, Hasan AM, Emara MM et al. Evaluating four synthesized Schiff bases as corrosion inhibitors on the carbon steel in 1 M hydrochloric acid. Corros Sci. 2012;65:67-76. DOI: https://doi.org/10.1016/j.corsci.2012.08.005
47. Musa AY, Kadhum AH, Mohamad A et al. Experimental and theoretical study on the inhibition performance of triazole compounds for mild steel corrosion. Corros Sci. 2010;52:3331-3340. https://doi.org/10.1016/j.corsci.2010.06.002
48. Bouklah M, Hammouti B, Lagrenee M et al. Thermodynamic properties of 2,5-bis(4-methoxyphenyl)-1,3,4-oxadiazole as a corrosion inhibitor for mild steel in normal sulfuric acid medium. Corros Sci. 2006;48:2831-2842. https://doi.org/10.1016/j.corsci.2005.08.019
49. Singh AK, Quraishi MA. Effect of 2, 2′ benzothiazolyl disulfide on the corrosion of mild steel in acid media. Corros Sci. 2009;51:2752-2760. https://doi.org/10.1016/j.corsci.2009.07.011
50. Bentiss F, Lebrini M, Vezin H et al. Enhanced corrosion resistance of carbon steel in normal sulfuric acid medium by some macrocyclic polyether compounds containing a 1, 3, 4-thiadiazole moiety: AC. Corros Sci. 2009;51:2165-2173. https://doi.org/10.1016/j.corsci.2009.05.049
51. Amin MA, Ahmed MA, Arida HA et al. Monitoring corrosion and corrosion control of iron in HCl by non-ionic surfactants of the TRITON-X series – Part II. Temperature effect, activation energies and thermodynamics of adsorption. Corros Sci. 2011;53:540-548. https://doi.org/10.1016/j.corsci.2010.09.019
52. Lebrini M, Bentiss F, Vezin H et al. The inhibition of mild steel corrosion in acidic solutions by 2, 5-bis (4-pyridyl)-1, 3, 4-thiadiazole: structure–activity correlation. Corros Sci. 2006;48:1279-1291. https://doi.org/10.1016/j.corsci.2005.05.001

53. Hoar TP, Holliday RD. The inhibition by quinolines and thioureas of the acid dissolution of mild steel. J Appl Chem. 1953;3:502-513. https://doi.org/10.1002/jctb.5010031105
54. Said M ElH, Bouraiou A, Bouacida S et al. 2-Hydroxymethyl-1, 3-dimethyl-1H-imidazol-3-ium triiodide. Acta Crystallogr. 2013;69:1340-1341. https://doi.org/10.1107/S1600536813022307
55. Mourya P, Singh P, Tewari AK et al. Relationship between structure and inhibition behaviour of quinolinium salts for mild steel corrosion: experimental and theoretical approach. Corros Sci. 2015;95:71-87. https://doi.org/10.1016/j.corsci.2015.02.034